Journal of Constructional Steel Research 67 (2011) 1386–1400

Contents lists available at ScienceDirect

Journal of Constructional Steel Research

journal homepage: www.elsevier.com/locate/jcsr

Numerical modeling of the fire–structure behavior of steel beam-to-column connections

Chen-Hung Lee [a,b,*], Yaw-Jeng Chiou [a,c], Hsin-Yang Chung [a], Chien-Jung Chen [b]

[a] Department of Civil Engineering, National Cheng Kung University, Taiwan
[b] Architecture and Building Research Institute, Ministry of the Interior, Taiwan
[c] National Center for Research on Earthquake Engineering, Taiwan

ARTICLE INFO

Article history:
Received 8 July 2010
Accepted 23 February 2011

Keywords:
Steel beam-to-column connection
Thermal analysis
Structural analysis
Fire dynamics simulator
Finite element method

ABSTRACT

This study proposes a numerical model to investigate the behavior of steel beam-to-column connections in fires. Two strategies have been employed to transfer thermal results from a fire simulation to structural analysis. A full scale fire test was performed on a steel beam-to-column connection following the ISO 834 standard fire curve; it was simulated to verify the proposed methods. The wall temperatures obtained by FDS were used as an interface for fire exposure on the surface of the structure. The numerical results are in agreement with the experimental data. In addition, the size effect of the furnace and a sensitivity analysis on insulation materials had been studied. Two reduced beam sections were analyzed and compared with the simulation results of an unreduced beam section. Both sections were able to withstand the severity of the blaze with the runway phenomenon occurred after a similar period of time for each beam.

1. Introduction

There has been considerable interest in the effects of fire on building structures over the few several years, motivated to some degree by the attack on, and subsequent collapse of, the World Trade Center (WTC) towers [1]. The collapse of the WTC towers showed that a greater understanding of how structures behave in fires is necessary.

Various methodologies and tools have been developed to study the interaction between fires and structural elements. Ghojel [2] proposed a simple heat transfer model to simulate real fires, based on the emission and absorption of radiation heat. It assumed that the structural elements in a compartment had no temperature gradient across or along the elements. Kuldeep et al. [3] presented a simple radiative transport model and assumed the compartment was locally divided into a hot upper layer and cool lower layer. A gap radiation model proposed by Ali et al. [4] assumed that the exposed portions of the structure were totally enveloped by hot gases during an ASTM E119 standard fire. Two dimensional structural finite element analysis was performed using the ABAQUS software. Wickstrom et al. [5] used adiabatic surface temperatures (AST) to present two new interfaces for the analysis of structures during fires. The concept of AST provided an efficient means of transferring thermal results from a fire simulation to a thermal/structural analysis. Duthinh et al. [6] showed that the computational methods could be enhanced to realistically study the effects of fires on buildings by using two new interfaces in fire-thermal-structural analysis. Recently, Kodur et al. [7] offered a macroscopic finite element to predict the fire response of reinforced concrete members, in the entire range: from the pre-fire stage to the collapse stage. At present, it is not easy to use the microscopic finite element based model to conduct a fire-thermal-structural analysis. The difference in spatial and temporal length scales, variation in numerical techniques, and the complicated nature of the related computer programs, all mean that analysis of structures during fires is very challenging.

At elevated temperatures the strength and stiffness of steel weakens, and the ability of the connections to withstand force during a fire directly affects the redistributed forces from the beams to other structural members. Iu et al. [8] presented a method for predicting the effect of heating and cooling on a multi-story frame in a real fire scenario and the temperature distribution in the frame was considered in both pre- and post-fire stages. Silva and Coelho [9] presented a model to evaluate the ductility of loaded steel connections. Al-Jabri et al. [10–14] carried out a series of studies of end plate steel connections at elevated temperatures. The results of the Cardington full-scale eight story steel building fire tests in the UK [15] have also shown how the connections help the structural system to survive extreme fires

* Corresponding author at: Department of Civil Engineering, National Cheng Kung University, 701 Tainan, Taiwan. Tel.: +886 6 2757575x.63145; fax: +886 6 2358542.
E-mail addresses: n6893101@mail.ncku.edu.tw (C.-H. Lee), ceyjc@mail.ncku.edu.tw (Y.-J. Chiou), hychung@mail.ncku.edu.tw (H.-Y. Chung), john@abri.gov.tw (C.-J. Chen).

0143-974X/$ – see front matter © 2011 Elsevier Ltd. All rights reserved.
doi:10.1016/j.jcsr.2011.02.014

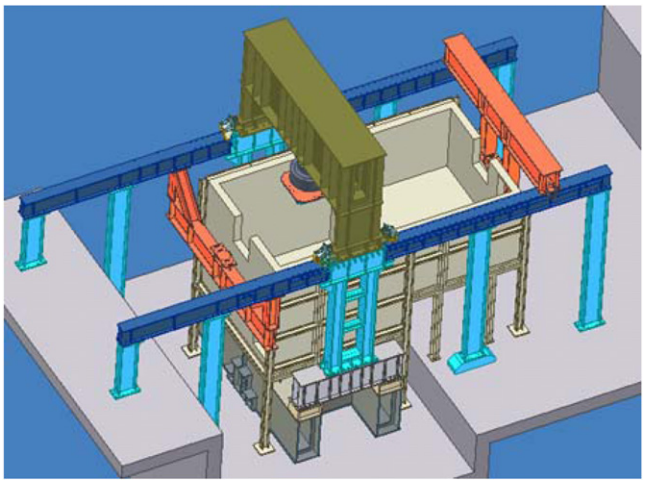

(a) Schematic configuration of test facility.

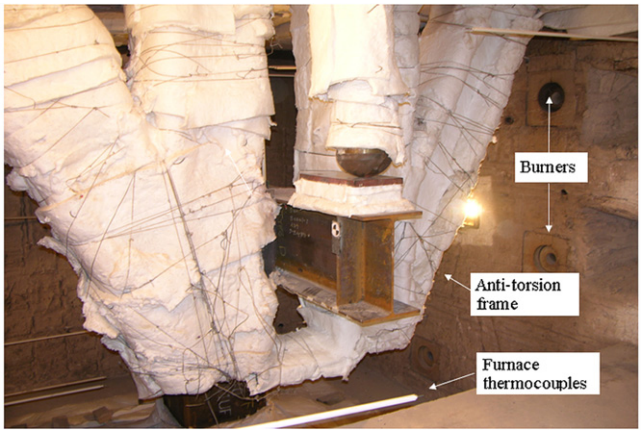

(b) The furnace thermocouples, burners and beam-to-column sub-frame.

Fig. 1. The test setup.

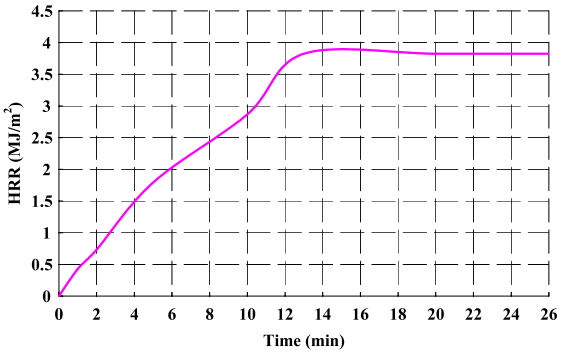

Fig. 2. Heat release rate for each burner in the furnace.

without progressively collapsing. Obviously, preventing beam-to-column connections from failing is important for steel structures subjected to fire.

This paper developed a methodology that could be used to assess the boundary conditions between the fire simulation and structural elements. Due to the complexity of realistic fire scenarios, this paper first focused on a standard furnace experiment with fuel and ventilation control systems, instead of a compartmental fire. The time–temperature curve of ISO 834 was adopted for the test. Wall temperatures obtained from FDS [16] were used as a medium for fire exposure on the structural elements. Data transfer between the computational fluid dynamics fire model (FDS) and the finite element thermal and structural model (ABAQUS) was established. This was useful for determining the temperatures on the exposed surfaces of the structural elements, for further finite element analysis. In addition, the size effect of the furnace and sensitivity analysis on insulation materials had been studied. Two cases with reduced beam sections had been analyzed to find the ability of fire resistance under the standard fire. These illustrations show how the proposed methodology can enhance the capability of computational methods used to study the effects of various steel members/connections in standard fires.

2. Transferring the boundary conditions of the fire–structure

FDS is a fire simulation that can be used to predict gaseous phase temperatures and solid phase temperatures at boundary conditions. Wall temperatures at boundaries can be calculated using the version 5 of NIST FDS. The results of the fire model can be used as input variables for detailed heat transfer calculations within a solid structure, by finite element (ABAQUS) analysis.

As defined by FDS, a one dimensional heat transfer calculation is performed at each solid boundary cell. Let $T_{s,i}$ indicate the temperature at the center of the i-th cell, and the wall temperature is defined as Eq. (1).

$$T_w \equiv T_{s,1/2} = \left(T_{s,0} + T_{s,1}\right)/2. \tag{1}$$

In order to transfer the solid surface boundary temperatures (T_w) from the FDS analysis to the FE analysis, it is necessary to create the corresponding nodes in both models. In the FEM grid system, the numbering of elements and nodes is required, but FDS does not have a node numbering function. This study therefore used ABAQUS to create and number the nodes used by FDS. The boundaries refer to the surfaces of the model, and the coordinates of all nodes at the boundaries are attached to the parameter wall temperature in the command of DEVC in FDS. The DEVC can be used to record some aspects of the simulated environment, such as thermocouples. The inner nodes of the model do not need to be assigned in the FDS simulation, because a one dimensional heat transfer calculation is performed at each solid boundary cell. The temperature profile is modeled for transient heat analysis in ABAQUS to determine the temperatures in each section of the model.

Two strategies were used to establish fire–structure interfaces. First, wall temperatures were obtained directly from the results of the FDS simulation and used as the boundary conditions for thermal analysis of the solid structure. This was done by assigning the temperatures from FDS to the boundary of the exposed surface of the solid structural members based on the same location and heated directionality. Second, transient thermal analysis in the FE model was performed by transferring the time-dependent temperature profiles, which had been derived from the FDS, predicted wall temperatures on the boundaries, to ABAQUS. A Matlab subroutine created by the authors was used as a tool for transferring the FDS wall temperatures to ABAQUS input.

3. Summary of experimental program [17]

This study adopted one of the experimental results, which were conducted by the Architecture and Building Research Institute (ABRI) in Taiwan, to verify the numerical solutions. The experimental procedures are summarized in this section. More details of this experiment can be found in [17].

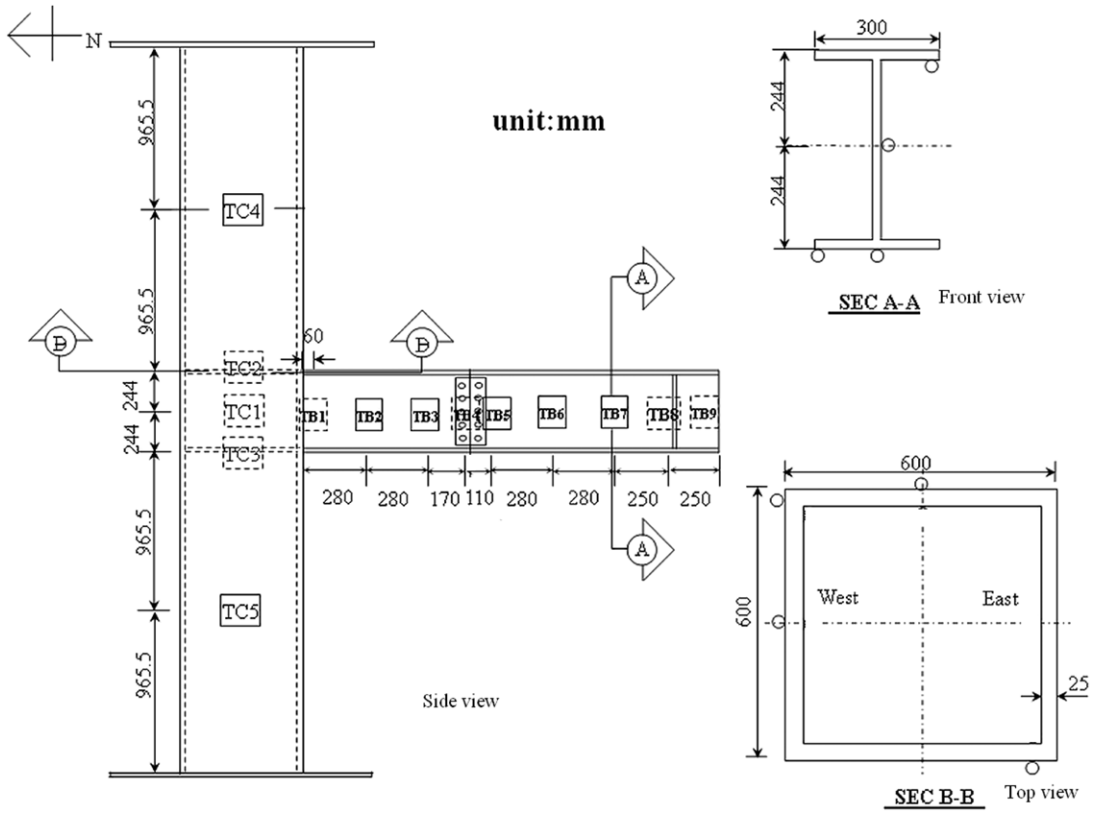

(a) K-type thermocouples.

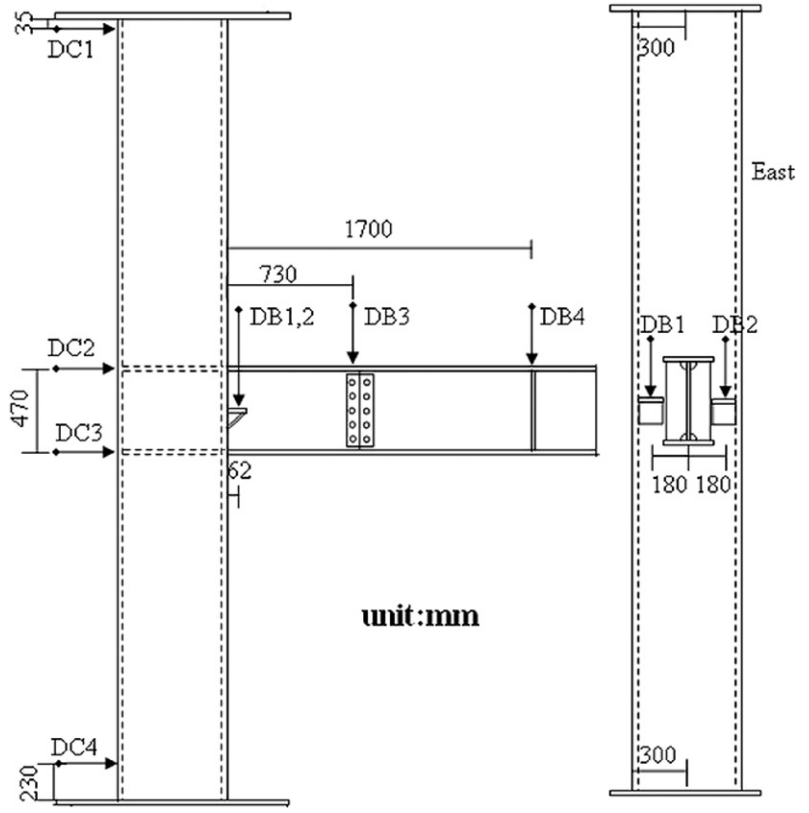

(b) Displacement transducers.

Fig. 3. Measurement instrumentation.

A full scale test of steel beam-to-column connections, under the ISO 834 standard fire curve, was adopted. The test facility, as shown in Fig. 1(a), was a multi-functional fire resistance test furnace that was capable of running fire resistance experiments for beam, column, and composite beam-to-column elements. Thirty burners were located on both sides of the walls and a pre-mixed gaseous system was used as the heat source, with propane as fuel. Gaseous temperatures were measured using twenty one horizontal furnace thermocouples (Fig. 1(b)) and all of the thermocouples were 100 ± 50 mm from the exposed face of the test specimen. The heat release rate per unit area of each burner is presented in Fig. 2. Fifty six K-type thermocouples, which can resist high temperatures of up to 1260 °C, were attached to the specimen for measurement of temperature, as shown in Fig. 3(a). The air flow caused two vents in the furnace to open, thereby maintaining the airflow rate at a constant velocity of 3 m/s during the test. The initial air temperature was measured at 28 °C.

The sections of the column and beam were 600 × 600 × 25 mm and 488 × 300 × 11 × 18 mm, respectively. The box column of the specimen was set in the center of the column furnace with its two ends connected to the bottom 2000 ton actuator and the top portal frame through ball-bearing plates. Ball-bearing plates at either end of the box column were utilized to generate hinge boundary conditions. The H-beam of the specimen stuck out into the beam furnace and was laterally braced by a moveable steel frame, and this anti-torsion frame was surrounded with fire resistant insulation to insure that it could offer enough strength to prevent lateral torsion buckling. Before the fire test, the box column was loaded with a constant 500 ton compressive load, and the cantilevered H-beam was then point-loaded 1.7 m away from the face of the column flange with a downward constant load of 36.8 tons. The amount of loading could reach 60% of the plastic moment at the connection.

As shown in Fig. 3(b), eight displacement transducers divided into two groups, DB- and DC-groups, were employed to observe the structural deformation of the combined specimen in the fire test. The DB-group displacement transducers (DB1–DB4) were utilized to measure the vertical deformations of the H-beam. The DB4 displacement transducer was placed at the same location where the beam load was applied. The DC-group displacement transducers (DC1–DC4) were distributed from the top to the bottom of the column. The DC2 and DC3 transducers were used to measure the deformations contributed by the rotation of the beam-to-column connection and panel zone deformation. All of the displacement transducers were firmly mounted outside the furnace, and contacted the measurement points of the specimen with extended ceramic rods inside the furnace. The expansion of the ceramic rods at elevated temperatures was calibrated prior to testing.

On calculating the relative rotation of beam–column joint, if the rigid body motion is neglected, the beam deflection is mainly caused by three components, the shear deformation at the panel zone, flexural deformation of the column and beam. Because the column of the test specimen was stocky, the flexural deformation of the column has been ignored. The method presented by AI-Jabri et al. [13] was adopted to define the relative degree of rotation between the beam and column. The rotation of the beam and column were defined as $\phi_b = \tan^{-1}(DB_3/1030)$ and $\phi_c = \tan^{-1}((DC_2 - DC_3)/470)$, respectively. The relative rotation of the connection was thus equal to $\phi_b - \phi_c$.

4. Numerical modeling

A virtual furnace was proposed to create the flow under fire curve ISO 834 to model the beam-to-column connection in the fire. In the FDS analysis, one mesh was used in the simulation and consisted of 216 000 (or 90 × 48 × 50) computational cells. The model, including the anti-torsion frame, was created using the OBST group, as was the furnace. The name list group OBST contained parameters used to define obstructions. Each OBST line contains the coordinates of a rectangular solid within the flow domain. The solid is defined by two points ($x1, y1, z1$) and ($x2, y2, z2$) that are entered on the OBST line in terms of the sextuplet $XB = x1, x2, y1, y2, z1, z2$. The major concern in FDS is that the model elements be located at the same coordinates which were created by ABAQUS. The VENT group was used to model two outlets adjacent to external walls of the furnace. The vents were chosen in a similar manner to the obstructions, with the sextuplet XB denoting a plane abutting a solid surface. Two of the six coordinates had to be the same; denoting a plane as opposed to a solid.

In order to compare the measured temperature of gaseous with the predicted data, 21 thermocouples were input into the FDS data. The locations of the thermocouples are illustrated in Fig. 4. The horizontal and vertical spaces of the thermocouples were 1.4 m and 1.2 m.

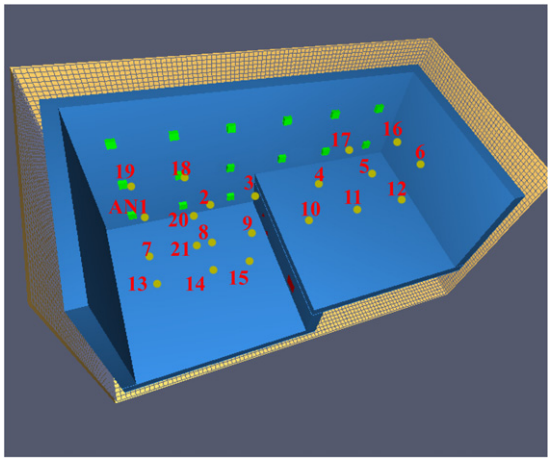

Fig. 4. The location of the furnace thermocouples (the circle point) in the simulation of FDS.

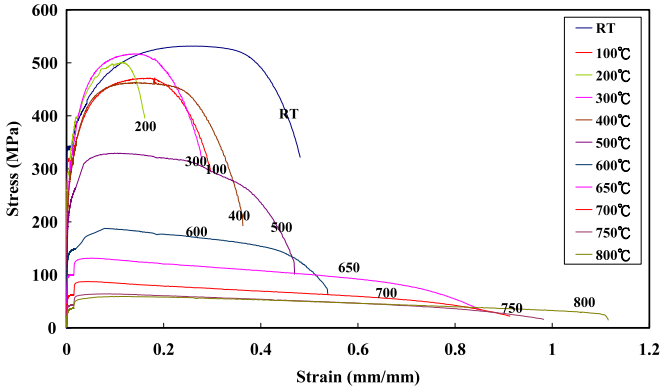

Fig. 5. The stress–strain curves at different temperatures.

Table 1
The friction coefficient of bolts at elevated temperatures.

Temperature (°C)	Friction coefficient
28	0.33
200	0.27
400	0.25
600	0.35
800	0.83

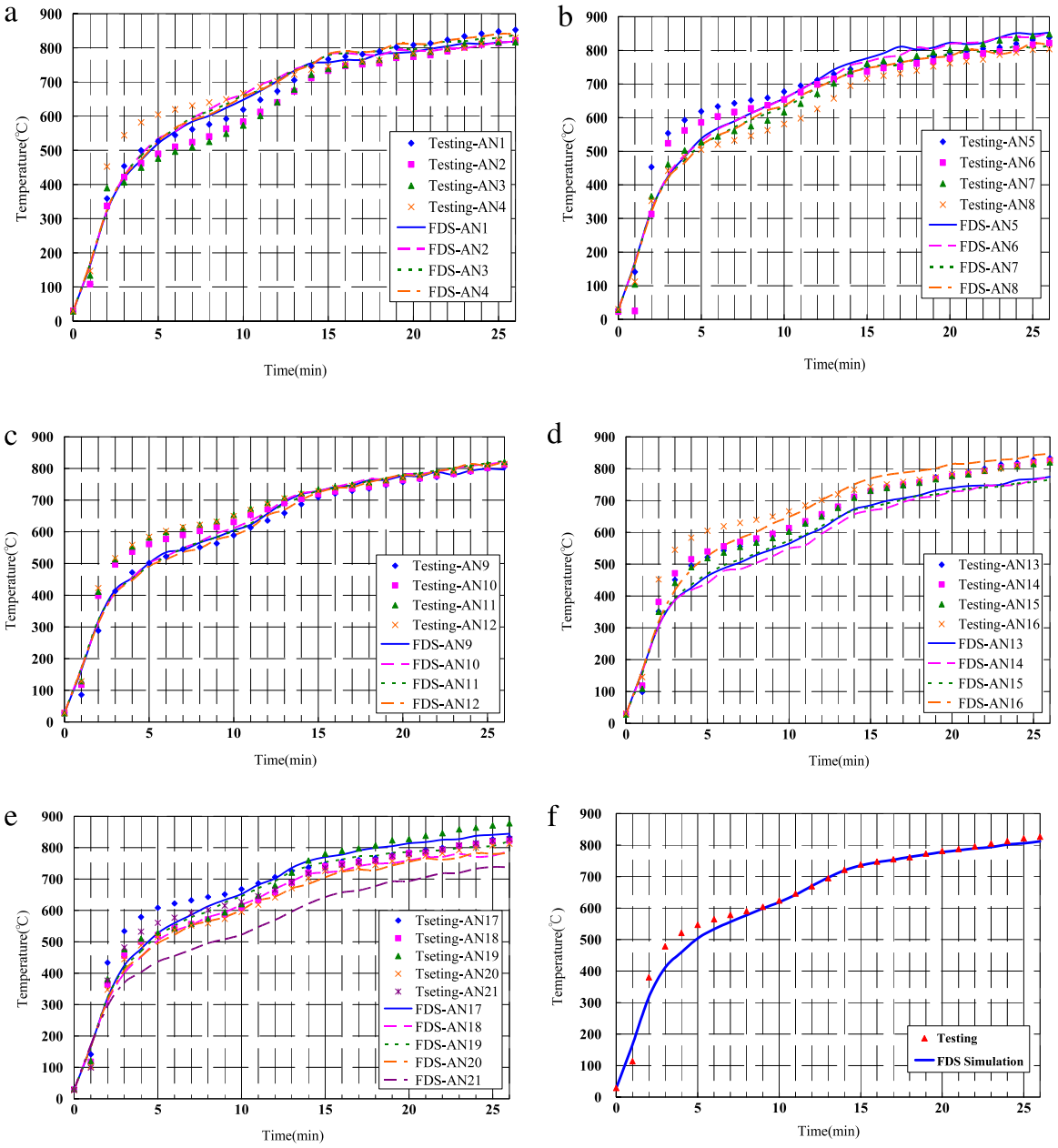

Fig. 6. Comparison of the measured and predicted gas temperatures in the furnace.

The walls of the furnace were made of fire-resistant fiber blocks with a thickness of 0.3 m and the following material properties: a specific heat of 1.05 kJ/kg K, the thermal conductivity of 0.12 W/m K and density of 500 kg/m^3. For the steel model, the thermal conductivity and specific heat were both temperature dependent, and determined from Eurocode 3 [18]. The density of the steel was considered independent of the temperature and taken to be $\rho_s = 7850$ kg/m^3.

A total of 8617 nodes were attached to the surface of the model to measure the boundary temperatures. The FDS simulation wall temperature results were input into an ABAQUS file. An eight-node linear heat transfer brick (DC3D8) was used to simulate the entire model for transient heat analysis, and the consequent file produced by the transient heat analysis was adapted for the non-linear structural analysis.

For the non-linear structural analysis, a three-dimensional FEM was created using the ABAQUS software. Sarraja et al. [19] used a complex model which accounted for material and geometric

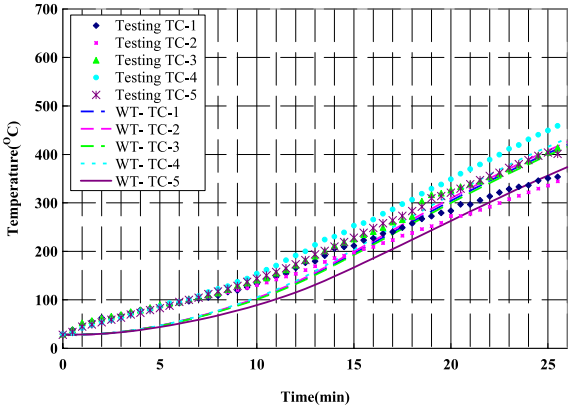

Fig. 7. Predicted (solid lines) and measured (symbols) average temperatures (°C) on TC1-5 as a function of time (min).

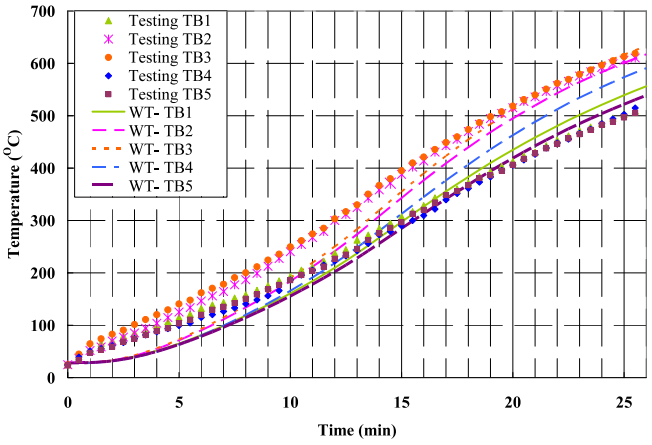

Fig. 8. Predicted (solid lines) and measured (symbols) average temperatures (°C) on TB1-5 as a function of time (min).

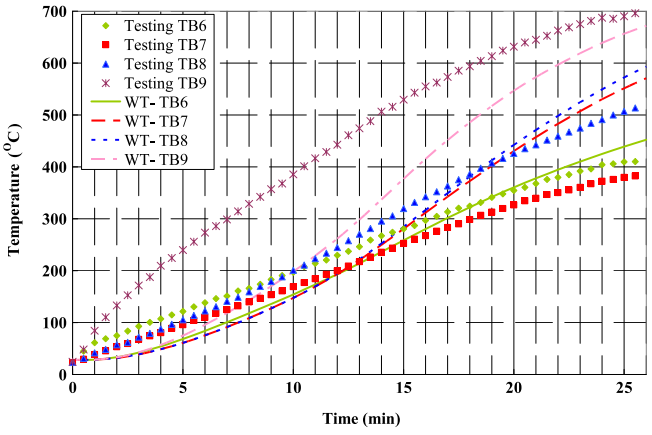

Fig. 9. Predicted (solid lines) and measured (symbols) average temperatures (°C) on TB6-9 as a function of time (min).

non-linearity, large deformation and contact behavior of steel fin plate connections. This study achieved a close agreement between the analyses and experimental results. It is clear that FEM was a reliable technique when used to predict the behavior of joints at elevated temperatures with an acceptable degree of accuracy.

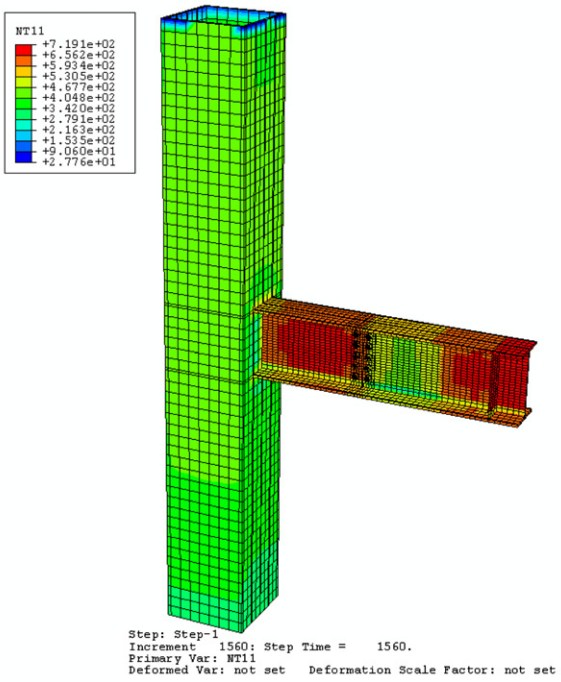

Fig. 11. Temperature results (°C) from thermal model at $t = 26$ min.

In this paper, the entire beam-to-column connection was modeled using eight-node continuum hexahedral brick elements (C3D8I) including the column, beam, bolts and plates. The material properties of stress–strain relationship for steel depend on the results of coupon test as shown in Fig. 5. Strain hardening has been taken into consideration in the simulation. At the connection, the beam was tied along its edge to simulate its having been welded to the column intersection.

In order to accurately capture the stress behavior in the region around the bolt holes where failures would most likely begin, an intensive mesh was made within the vicinity of the bolt holes. The bolt holes were modeled as 3 mm larger than the bolt shank

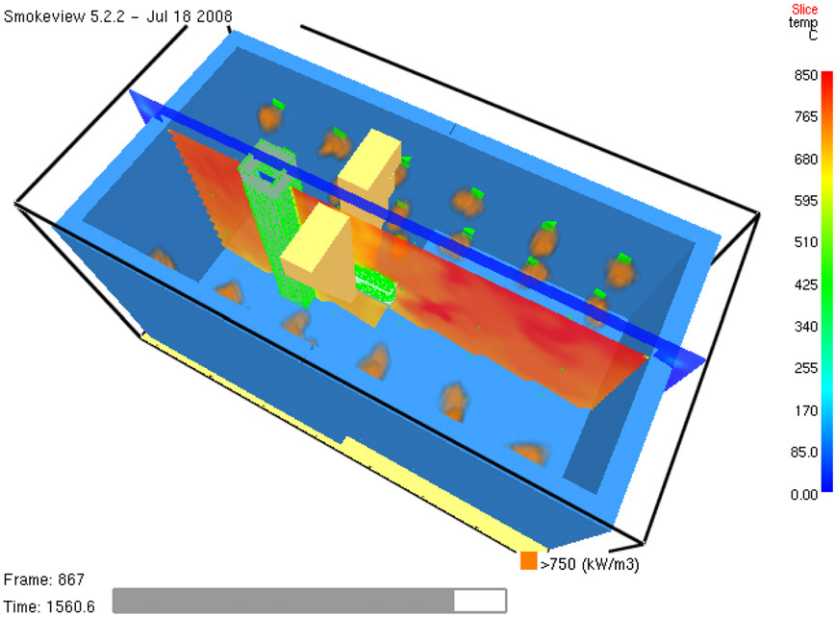

Fig. 10. FDS representation of the gas temperatures profile in the furnace.

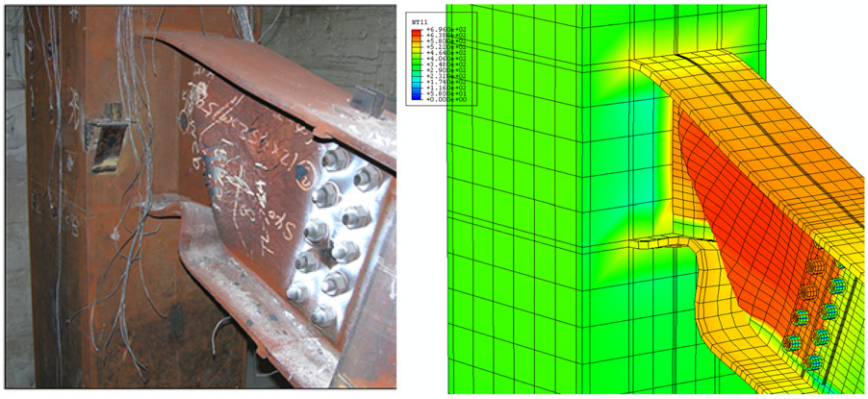

Fig. 12. The failure mode of the experiment and simulation result in fire.

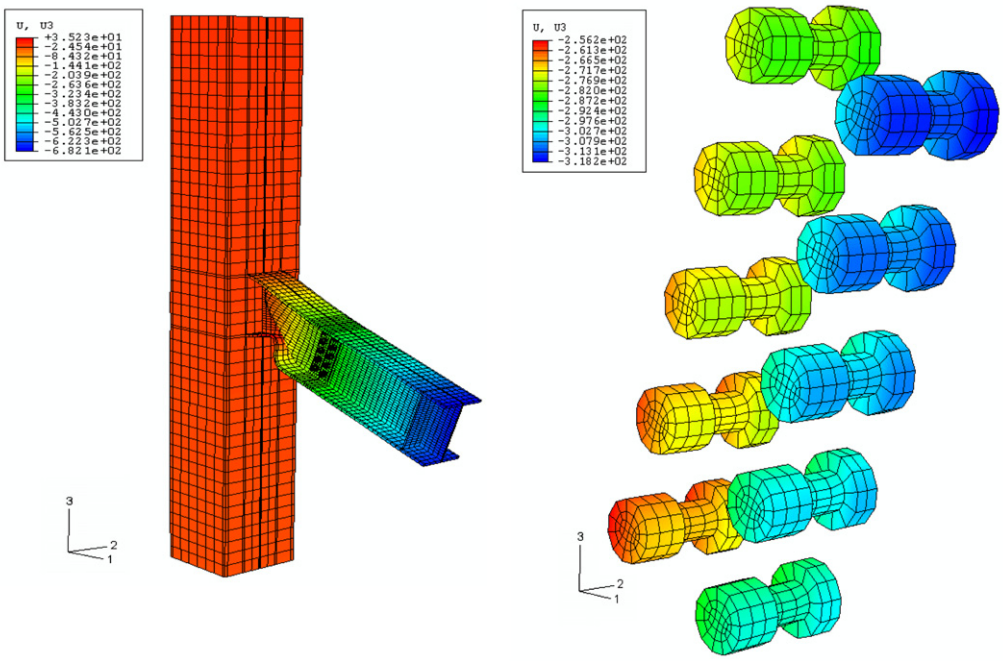

Fig. 13. The predicted deformations of the beam-to-column connection and bolts.

diameter. Each bolt was restrained only at the reference point which was located at the center of the bolt head, preventing horizontal movement, and then for the next analysis step all bolts were freed of any restraints, as contact had already been established. To transfer the load fully, surface-to-surface contact and small-sliding were used for all contacting surfaces which allow large rotations of the surfaces, as long as the surfaces do not move significantly relative to each other. The contact areas in the beam web connection were comprised of bolt shank-to-bolt holes, bolt head-to-plate, nut-to-plate and plate-to-beam web surface. The master surfaces included the bolt shank, bolt head, and nut (as the bolt was of stiffer material), and all the other contact surfaces were considered slaves. During the analysis, the bolts were preloaded using the command 'bolt load' in ABAQUS. Friction between the contact surfaces at the connection was modeled using the classical Coulomb model. The friction coefficient was temperature dependent and taken as 0.33 at ambient temperature in Table 1. The friction coefficient decreased gradually with raised temperature in 400 °C. When the temperature was over 400 °C, the surface of steel member became soft and rougher. Nearby the steel plates also had an enormous lateral force to tie the plates to extrude inward. Between the steel plates there was a linking phenomenon occurrence and then the friction coefficient increased with the higher temperature.

It is difficult to simulate the contact interaction between parts by using ABAQUS/Standard, and special procedures are needed to determine contact between the connecting parts. Specifically, while nodes on the master surface can penetrate slave surface segments; the reverse is not true. Therefore, the mesh should be fine enough for the node of each element on the master surface to face a corresponding node on the slave surface. In addition, the load should be applied slowly until contact is established. At the same time, any singularity problems at the boundary that may arise should be avoided to achieve accurate modeling.

5. Validation of the numerical model

Throughout this discussion, results from the FDS predictions were compared with gaseous and solid phase temperatures directly measured in the experiment. The simulation was run for the equivalent of 26 min real time. Each simulation required 40 h to compute. The temperature distribution of on the exposed surfaces of the beam-to-column connection from the analysis of FDS was transferred to the boundary conditions of the transient heat and structural analysis.

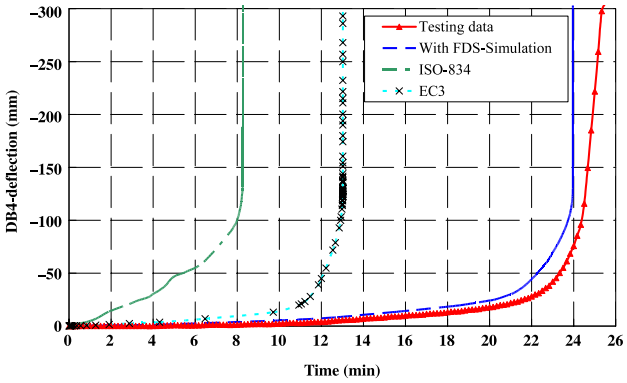

Fig. 14. Comparison of the FE simulation, EC3 code and test data of the time-deflection curves.

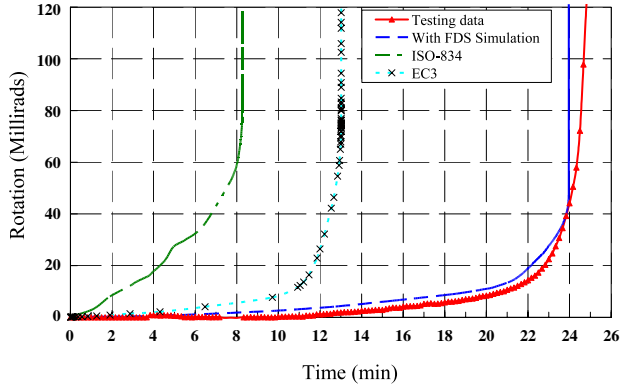

Fig. 15. Comparison of the FE simulation, EC3 code and test data of the time–rotation curves.

5.1. The gaseous-phase simulation

Results from the FDS predictions were compared with the measured temperatures. The heat release rate in Fig. 2 shows a very rapid increase during the first 13 min, and then there was a stable heat release rate modeled until the end of the simulation. These trends in the heat release rate were reflected in the predicted gaseous temperature distributions at various locations throughout the simulation. The predictions are depicted in Fig. 6(a)–(f). It can be seen in Fig. 6(a), in 15 min, the predicted gaseous temperatures of AN1, AN2 and AN3 have been overestimated when compared to the measured data. The predicted gaseous temperatures of AN5–AN8 were close to the measured data. As we can see in Fig. 6(c), in 10 min, the predicted gaseous temperatures were underestimated when compared to the measured data, but the final result were good. The numerical predictions of AN13–AN15 tend to be lower than the measured temperatures, as shown in Fig. 6(d). So does of AN21 in Fig. 6(e). The predicted average gaseous temperature was found to correspond to the measured average temperature throughout the duration of the experiment. The predicted average gaseous temperature increase in the first 6 min was very rapid. A strong correlation between the measured and predicted temperature was achieved from 6 to 22 min in Fig. 6. In addition, the predicted average temperatures were close to those measured at 26 min, (approximately 800 °C).

5.2. The solid-phase simulation

The temperature distribution on the column surface showed that TC4 had the hottest temperature, matching the measured data, and the predicted temperatures were lower than the measured ones during the first 10 min, as shown in Fig. 7. The numerical

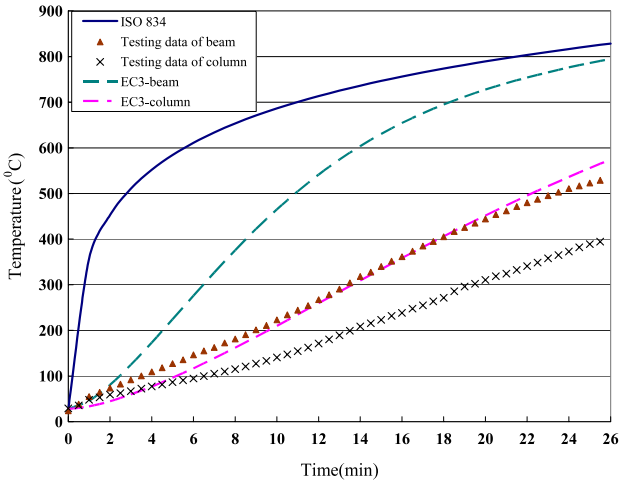

Fig. 16. Comparison of predicted and measured temperatures of the specimen exposed to ISO 834 fire.

predictions at location TB1–TB5 tended to be lower than the measured temperatures during the first 10 min, as shown in Fig. 8. At around 20 min, the simulation results matched the measured data very well. In Fig. 9, the measured temperatures at TB9 were higher than at other locations, which may imply that the *K*-thermocouples at TB9 were out of order. It should be noted that the anti-torsion frame caused additional turbulence, which may have affected the gaseous temperatures around it, causing the predicted temperatures (TB6–TB9) to deviate from the measured data. Fig. 10 shows the FDS representation of the gaseous temperature distributions within the furnace, showing the drastic spatial variations and concentrations in the maximum temperatures in the regions of interest.

The most important aspect of the experiment was how the time-dependent temperatures on the surfaces transferred to the structural analysis. All wall temperature (T_w) parameters were collected and put into the corresponding node locations to be the boundaries for transient heat analysis conducted using ABAQUS. A total of 8617 nodes were applied at boundaries. Fig. 11 shows the temperature contours for the beam-to-column connection, revealing that the temperatures had a continuous distribution; thus proving that the proposed method was valid.

5.3. Comparison of the structural behavior in fire

A comprehensive FE model combined with the FDS analysis, including bolts, was created to match the test conditions, even though bolt shearing was not the primary failure model studied in this test. The FE results were compared in terms of time–deformation characteristic at DB4, time-rotational characteristic at the connections, and the failure mode at the connections. Fig. 12 shows a comparison between the actual and predicted failure mode at the connections. There is some local deformation at the bottom of the flange where the beam was subjected to the highest compressive stress. This behavior was predicted by the FE model, as shown in Fig. 13. Shear failure on the bolts and plates did not occur in this test, indicating that the extended beam connection using bolts on the web had not significantly affected the results.

The time–deformation and time–rotation curves for the tested connection and the FE model that combined with the FDS simulation, as shown in Figs. 14 and 15, were compared; and showed reasonable agreement. Although there were a few small differences in the runaway stage, the point at which runaway began was nearly 24 min for both the test and the FE model. The

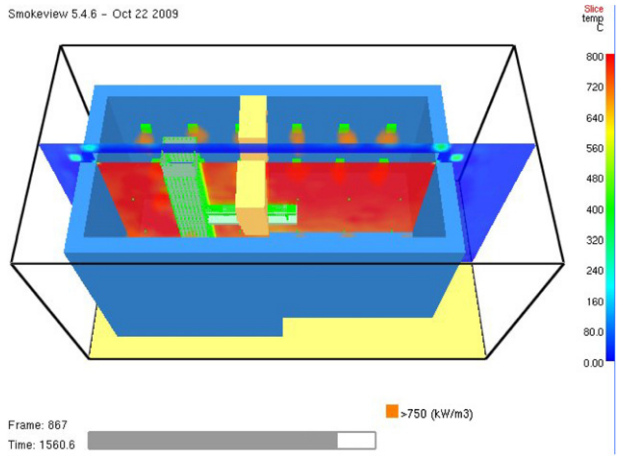

(a) The distribution of gas temperature for size factor = 0.8.

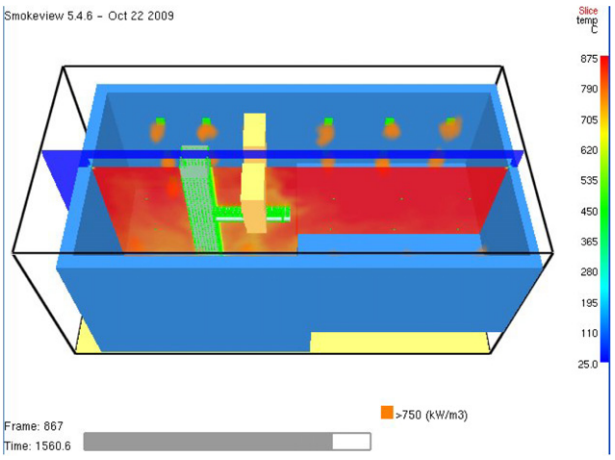

(b) The distribution of gas temperature for size factor = 1.2.

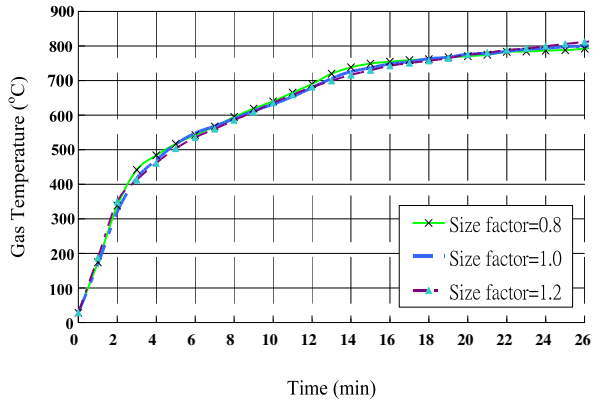

(c) The development of gas temperature in different size of furnaces.

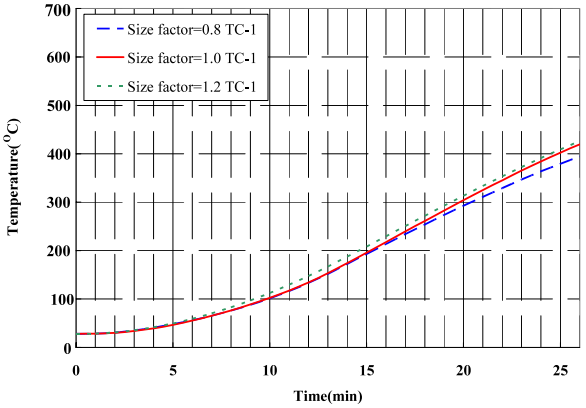

(d) Comparison of the surface temperature of column at TC1.

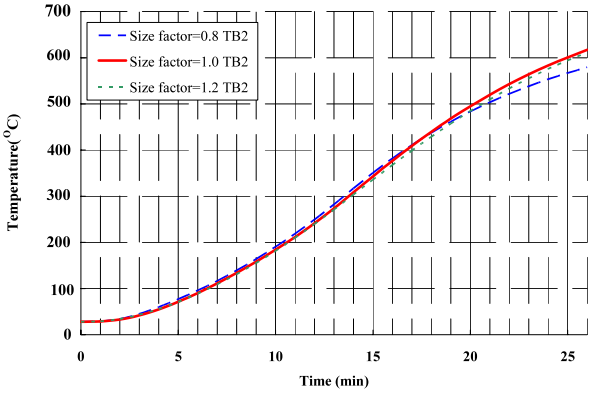

(e) Comparison of the surface temperature of beam at TB2.

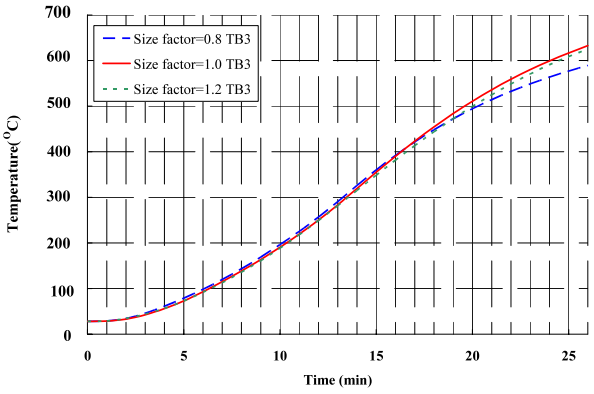

(f) Comparison of the surface temperature of beam at TB3.

Fig. 17. The simulation results of the different size of furnaces.

Table 2
Temperatures (°C) gained for a steel column with 24 mm ceramic fiber blanket insulation at the 60th minute of standard fire.

	FDS		EC3	
Temperature (°C)	$\lambda_p = 0.12$	λ_p = varies with time	$\lambda_p = 0.12$	λ_p = varies with time
$\varepsilon_{res} = 0.2$	165	154		
$\varepsilon_{res} = 0.5$	168	159	163	149
$\varepsilon_{res} = 0.7$	168	161		

small differences may be due to the complicated arrangement of the test, particularly with regard to the anti-torsion frame. In the FE model, a number of nodes on the flange were restrained by fixing their horizontal displacement, but in reality the anti-torsion frame deformed significantly due to the failure of the fire resistant insulation. Nonetheless, the model was still able to effectively predict the structural behavior in fire to a reasonable degree of accuracy. After 24 min, the strain increment had exceeded the

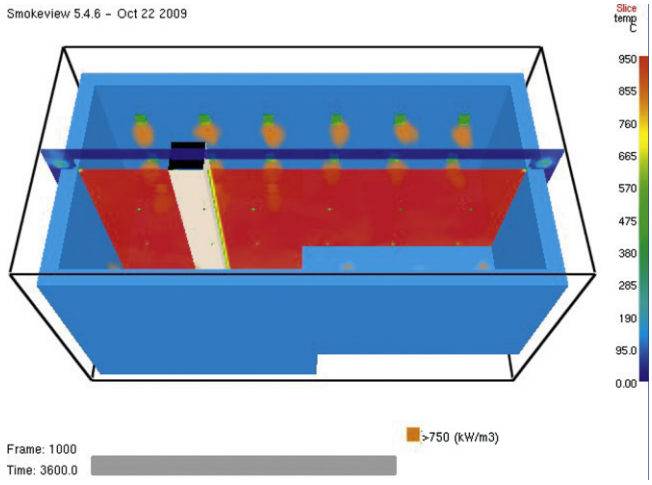

(a) The slice gas temperature at the furnace center.

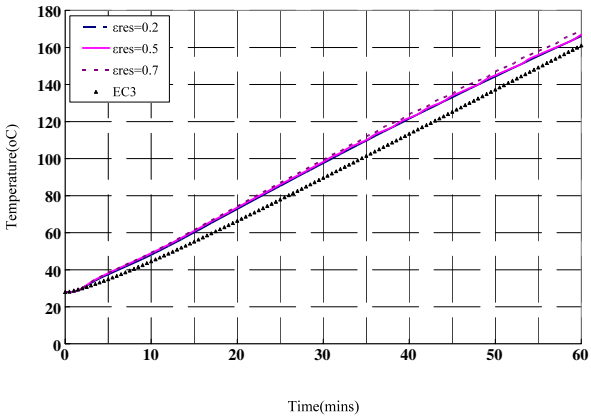

(b) Temperature–time history of a steel column with a constant value of λ_p.

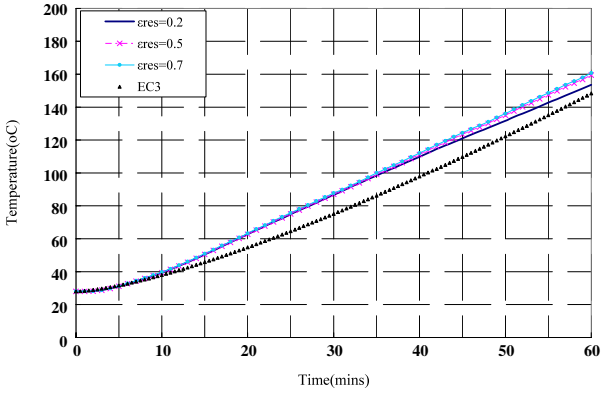

(c) Temperature–time history of a steel column with the true value of λ_p.

Fig. 18. Comparison of the temperature development of a steel column with the simulation results and EC3 code.

allowable value and failed to converge. Then the simulation was terminated.

Prior to the test, there was no sufficient data for temperature distribution on the surfaces of the model. The preliminary analysis of the beam-to-column connection subjected to a standard fire could be done by method (1) using gaseous temperatures as the uniform solid phase temperatures, and (2) different design codes. One of the famous standard fire curves is ISO 834 and the gaseous temperature is defined as in Eq. (2).

$$T_g = 345 \times \log(8 \times t + 1) + 20 \tag{2}$$

where t is the heating duration in minutes.

The design code of steel structures in fire such as Eurocode 3 [18] offered an equivalent uniform temperature in the cross-section, the increase of temperature ΔT_s in an unprotected steel member during a time interval Δt determined from the following equation.

$$\Delta T_S = \frac{F}{V}\frac{1}{\rho_s C_S}\left[h_c\left(T_f - T_s\right) + \sigma\varepsilon_{\text{res}}\left(T_f^4 - T_s^4\right)\right]\Delta t \tag{3}$$

where F is the surface area of unit length of the member, V is the volume of steel in unit length of the member. In this case, the values of F/V were equal to 41.74 and 136.57 (m^{-1}) of column and beam respectively. The convective heat transfer coefficient h_c was recommended to have a value of 25 W/m^2 K for the standard fire. σ is the Stefan–Boltzmann constant (5.67×10^{-8} W/m^2 K). The value of resultant emissivity ε_{res} has been defined in ENV 1991-2-2 and could be taken as 0.5. T_f is the temperature in the fire environment, and T_s is the temperature of steel. The calculation method is based on the principle that the heat entering the steel over the exposed surface area in a small step Δt is equal to the heat required to raise the temperature of the steel by ΔT_s assuming that the steel section is a lumped mass at a uniform temperature.

It was very obvious that the temperature predictions on steel by EC3 were higher than the test data on the beam and column as shown in Fig. 16. The result of preliminary analysis indicated that the connections failed quickly and the runaway phenomenon occurred at about 8 and 13 min by method (1) and (2), as shown in Figs. 14 and 15. The result was completely different from the test data and the analysis combined with the FDS simulation. It is obvious that using the FEM combined with the FDS simulation could be an effective method to analyze the behavior of structures with beam-to-column connections in fires. On the other hand, the results show that designing from the EC3 code is more conservative.

5.4. The size effect of the furnace

The results from Wong [20] showed that the thermal response of steel members in fire was affected by the compartment size. This study adopted two different sizes of furnace to study the size effect on temperatures of the structural steel in a standard fire. A reduction of 0.8 times (size factor = 0.8) and enlargement of 1.2 times (size factor = 1.2) in length and width of the former

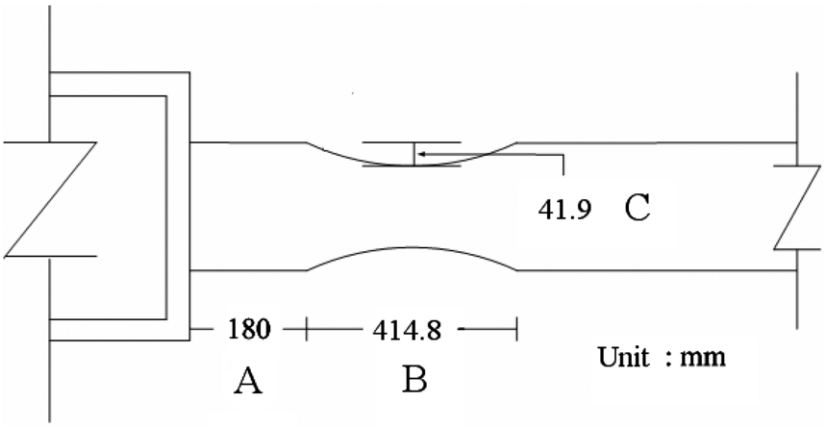

(a) DMC.

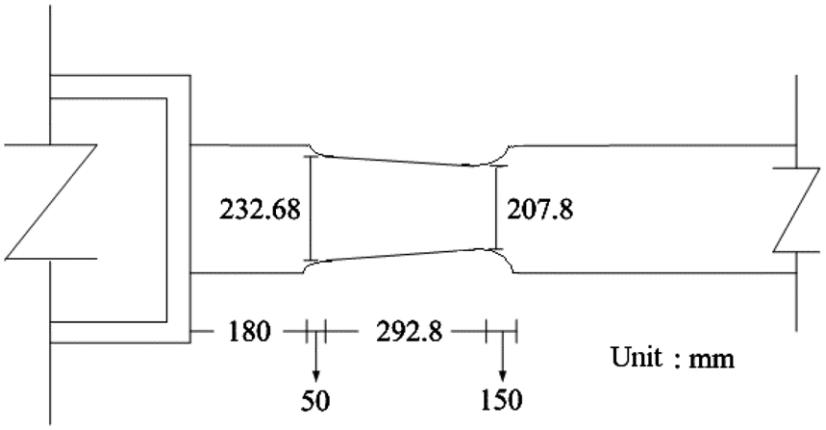

(b) DSMC.

Fig. 19. The dimensions of DMC and DSMC simulated in the model.

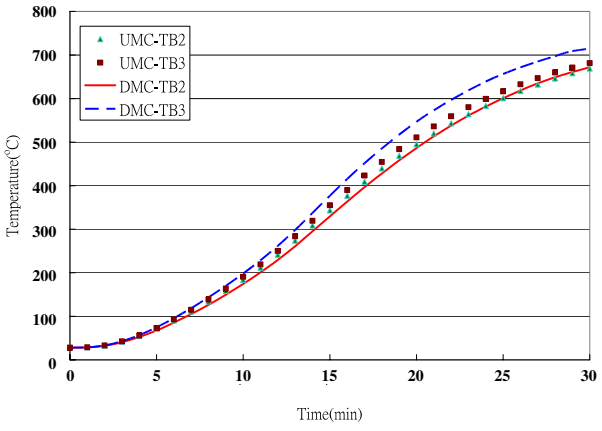

(a) The average temperatures (°C) of DMC (solid lines) and UMC (symbols).

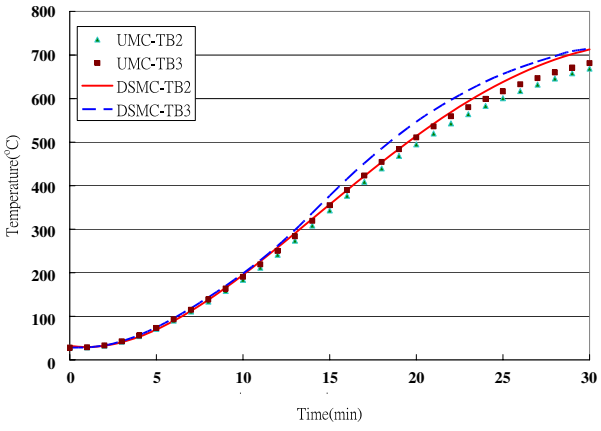

(b) The average temperatures (°C) of DSMC (solid lines) and UMC (symbols).

Fig. 20. The average temperatures (°C) of UMC, DMC, and DSMC on TB2&3 as a function of time (minute).

virtual furnace had been modeled by using the proposed method (Fig. 17(a) and (b)). The gas temperature meant the average temperature of all the thermocouples which were 100 mm from the exposed face of the steel members. The dimensions of the steel members were all the same as those in Section 3.

The development of gas temperatures are shown in Fig. 17(c). One can see that the development of gas temperatures are quite close for the different size of furnaces. The solid-phase temperatures on the surface of steel members are depicted in Fig. 17(d)–(f). Obviously, the surface temperatures on the column at TC1 were similar for different size factors, and so did TB2 and TB3. Even though the distance between specimen and furnace wall had been changed, the proper heat release rate of each burner still led the average gas temperature to follow the ISO 834 standard fire curve. Therefore, the radiation reflects from the surrounding material of furnace, would not be the major factor

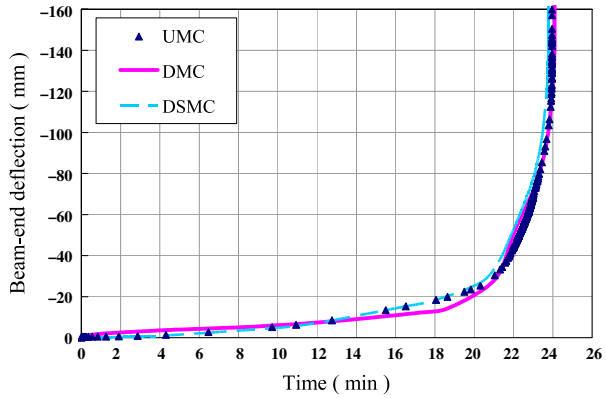

(a) The deflection curve varies with time.

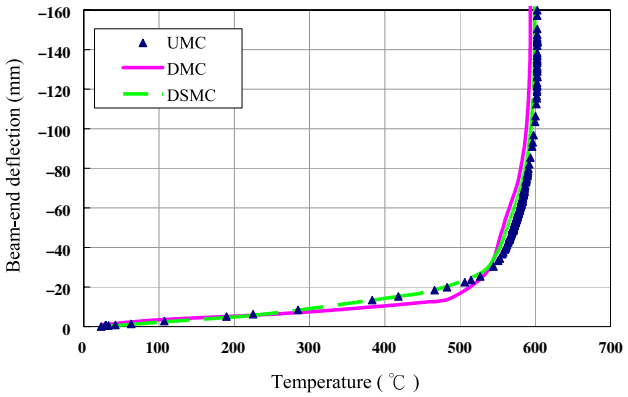

(b) The deflection curve varies with temperature.

Fig. 21. The analyzed result of the deflection curves at DB4.

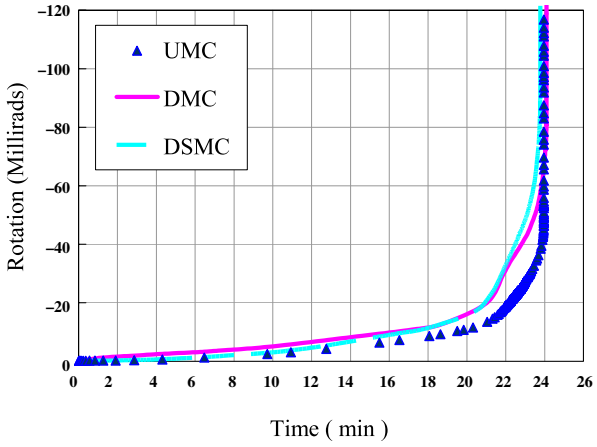

(a) The rotation curve varies with time.

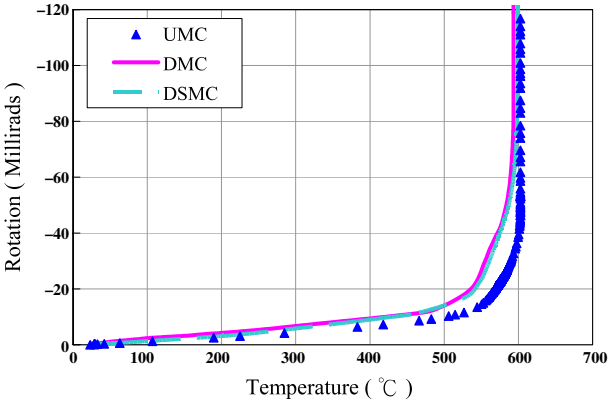

(b) The rotation curve varies with temperature.

Fig. 22. The analyzed result of the rotation curves at the connection.

which influenced the development of solid-phase temperatures in the full-scale standard fire.

5.5. Sensitivity analysis

The factors of the EC3 formula for the temperature prediction of protected steel member were adopted for the sensitivity analysis. A similar study was presented by Wong and Ghojel [21]. A ceramic fiber blanket with thickness 24 mm was used for insulation material. This EC3 formula is given as follows.

$$\Delta\theta_{a,t} = \frac{\lambda_p A_p/V}{d_p c_a \lambda_a} \frac{(\theta_{g,t} - \theta_{a,t})}{(1+\phi/3)} \Delta t - (e^{\phi/10} - 1)\Delta\theta_{g,t} \quad (4)$$

where

$$\phi = \frac{c_p \rho_p d_p}{c_a \rho_a}(A_p/V),$$

$$c_p = 820\ \mathrm{J/kg\,^\circ C}, \qquad \rho_p = 96\ \mathrm{kg/m^3},$$

$$\lambda_p = 0.033\text{–}1.443 \times 10^{-8}\theta_{a,t} + 2.875 \times 10^{-7}\theta_{a,t}^2\ \mathrm{W/m\,^\circ C}$$

c_a is the specific heat of steel, c_p is the specific heat of the insulation, d_p is the thickness of insulation, $\theta_{a,t}$ is the steel temperature at time t, $\theta_{g,t}$ is the ambient gas temperature at time t, λ_p is the thermal conductivity of the insulation, ρ_p is the unit mass of the insulation, ρ_a is the unit mass of steel.

The temperature of box steel column with cross-section 600 × 600 × 25 mm and high 4350 mm was studied. The surface temperature of column meant the average temperature at the typical thermocouple positions required in the ISO 834-7 standard. In a standard fire of 60 min, the temperatures attained by the steel column using different parameters were shown in Table 2 and Fig. 18. From Table 2 and Fig. 18, one can see that there was not much difference in the temperature gained by the column of the value of ε_{res}, where ε_{res} was the emissivity product of the fire and steel member. The maximum difference surface temperature when using FDS is only 7 °C between the result when $\varepsilon_{res} = 0.7$ and $\varepsilon_{res} = 0.2$. It showed that value of ε_{res} was not a significant parameter when predicting the surface temperature of a steel member through a layer of insulation. The more significant difference in the results is the use of the temperature dependent λ_p in comparison with the constant λ_p of 0.12. The maximum difference surface temperature when using FDS simulation is 11 °C and 14 °C from the calculation of EC3 formulation. From the sensitivity analysis of this study, it had found that for insulation with low density and low conductivity, the FDS simulation gave reasonable results comparable to the EC3 formulation.

6. Application of the analysis of structures during fires

The proposed method was applied to investigate the response of two beam-to-column connections with reduced beam sections to fires, including the dog-bone moment connection (DMC) and ductile seismic moment connection (DSMC). Except for the section of the beams that had been cut, the arrangement of the simulation was the same as in the model presented in Section 4. It includes the material properties at elevated temperatures, the dimensions

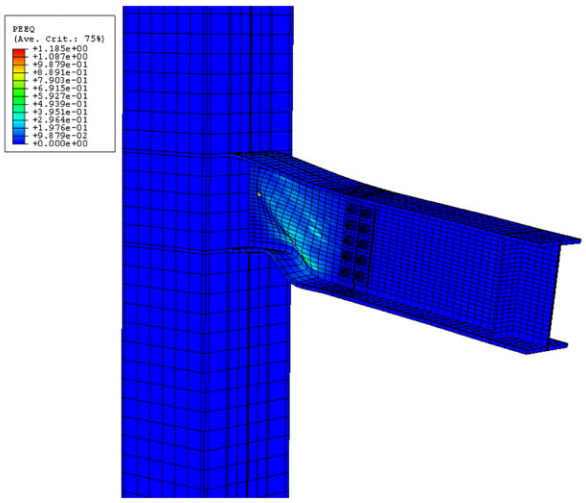

(a) The first yield region of UMC.

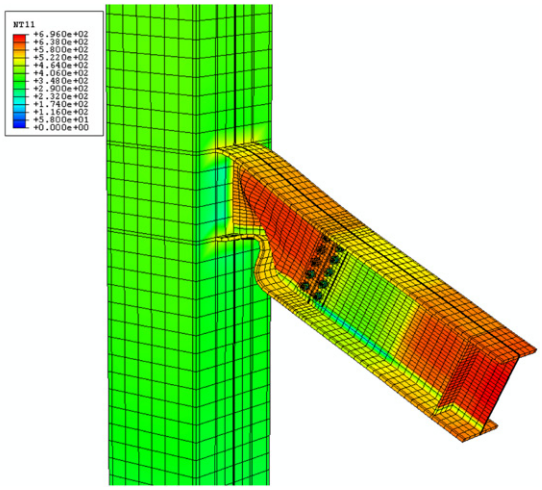

(b) The failure mode of UMC.

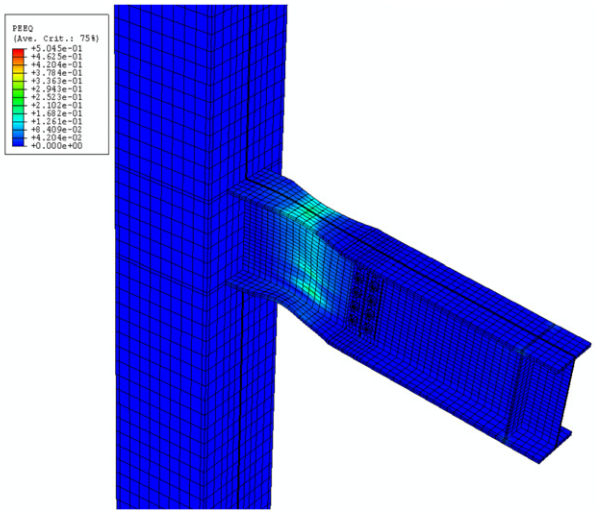

(c) The first yield region of DMC.

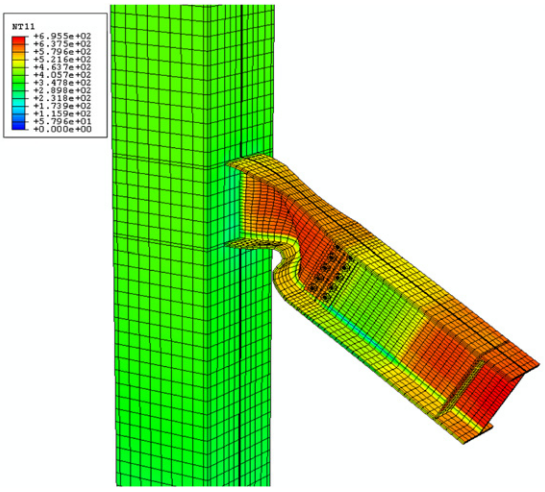

(d) The failure mode of DMC.

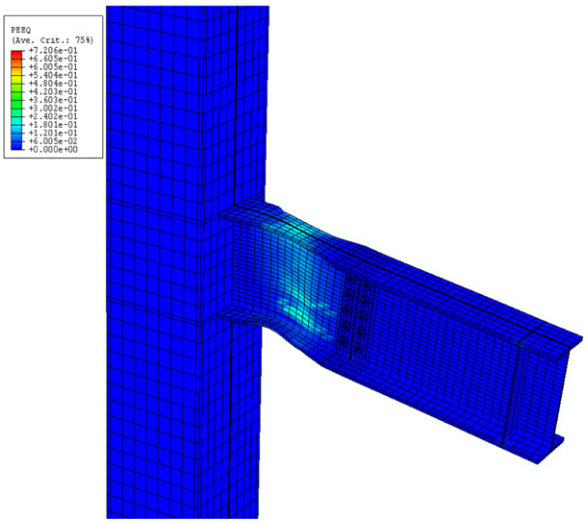

(e) The first yield region of DSMC.

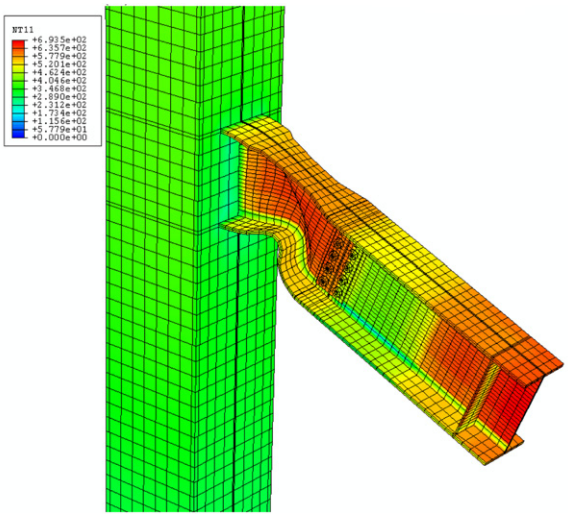

(f) The failure mode of DSMC.

Fig. 23. The first yield region occurred at the UMC, DMC and DSMC and their failure modes.

of the model, the heating duration and loading condition. For the convenience of comparing the result, the previous analysis in Section 5 was called an unreduced moment connection (UMC).

6.1. The dog-bone moment connection subjected to fire

Referring to Fig. 19(a), the key dimensions for the radius cut dog-bone [22] include the distance from the face of the column to the start of the cut (dimension *A*), the length of the cut (dimension *B*), and the depth of the cut (dimension *C*). In this case, approximately 28% of the beam flange width was removed. The stiffness reduction of the DMC was 10% at room temperature. A total of 8428 nodes were attached to the surface of the DMC to receive the boundary temperatures in FDS. Due to the section of beam having been cut; the temperatures at sections TB2 and TB3 were somewhat different than with the UMC. The width of the flanges was shorter and the process of heat transfer had become quicker on DMC. It is obvious that the temperature at TB3 of DMC is higher than those of UMC and the temperatures at TB2 were similar in Fig. 20(a).

At room temperature, the stiffness of DMC was less than for the UMC. The temperature distribution at the cut area was higher than at the UMC. The response of the DMC in fire may have been weak. When the deflection at DB4 and the rotation at the beam-to-column connection were compared (Figs. 21 and 22), the runaway trend indicated that the behavior of DMC was close to that of the UMC during the fire. The time and temperature of runway circumstance at DB4 were 24.03 min and 595 °C for the DMC, 24 min and 602 °C for UMC. For the rotation at the beam-to-column connection, the time and temperature of runway circumstance were 24.08 min and 589 °C for DMC, 23.98 min and 601 °C for UMC. Even so, the first yield region of the UMC and DMC were different, according to the analysis results. As can be seen in Fig. 23(a) and (c), the yield regions mainly occurred at the web of the UMC and top flange and web of the DMC. The failure modes were local buckling at the bottom of the flange and web buckling as shown in Fig. 23(b) and (d). The local buckling happened at the DMC which was further from the surface of the column than with the UMC. It also indicated that the critical moment occurred at the section was lower than that of the UMC. That is probably why the DMC carried higher surface temperatures but the deflection at the beam and the rotation at the connection were very close to the results from the analysis of UMC.

6.2. The ductile seismic moment connection subjected to fire

The design of the DSMC referred to the Ref. [23], as shown in Fig. 19(b), and a maximum of 30% of the width of the beam flange was removed. The reduction in stiffness in the DSMC was 9% at room temperature. A total of 8318 nodes were attached on the surface of the DSMC to measure the boundary temperatures in FDS. The temperatures at TB2 and TB3 of DSMC were higher than those of UMC, as shown in Fig. 20(b). Comparisons of the temperatures at TB2 of DMC and DSMC were quite similar. The temperature at TB3 of DSMC was higher than that of DMC.

In Figs. 21 and 22, the runaway trend indicated that the behavior of DSMC was quite close to that of the UMC and DMC during the fire. The time and temperature of runway circumstance at DB4 were 23.88 min and 600 °C of DSMC. For the rotation at the beam-to-column connection, the time and temperature of runway circumstance were 23.92 min and 600 °C of DMC. The first yield region of the DSMC occurred mainly at the top flange and web and the failure modes of both were the local buckling at the bottom of the flange and web buckling as shown in Fig. 23(e) and (f). Local buckling also occurred at the DSMC, which was further from the surface of the column than the UMC.

7. Conclusions

When the beam-to-column connections were subjected to standard fires, the exposed surfaces of the models were heated with time-dependent gaseous phase temperatures. Non-homogenous distribution of the solid phase temperatures took place on the surfaces of the model. Analysis combining the time-dependent gaseous and solid phase temperatures was required. Any assumption that the gaseous temperatures could be used to equate the distribution of solid phase temperatures on the models will necessarily underestimate the behavior of the beam-to-column connections in fire.

In this study, the behavior of beam-to-column connections were simulated and analyzed to illustrate a methodology for the calculation of the time to failure in fires. Via the wall temperatures, FDS was able to estimate the gaseous temperatures in the furnace and surface temperatures on the model. In the gaseous phase, the simulation results from the analysis of FDS agreed well with the measured temperatures from the thermocouple. In the solid phase, the predicted temperatures on the surface of the model were also close to the measured data.

When the transient heat transfer and structural analysis had been completed, the linear heat transfer bricks (DC3D8) and three dimensional solid elements (C3D8I) were used to model the beam-to-column connections. Contact behavior was also involved, and based on the Coulomb friction law. There was reasonable agreement between the predicted and measured responses at the deflection and rotation in both the elastic and plastic ranges. Furthermore, two cases were used to analyze the dog-bone moment connection (DMC) and ductile seismic moment connection (DSMC) when subjected to fire. By using the presented methodology with a virtual furnace, it was possible to predict the solid phase temperature distribution on the DMC and DSMC. Due to the fact that the flanges were narrower and the heat transfer was quicker, the temperatures on the reduced beam sections were higher than those before cutting the beam. Even for the sections of the beams that had been cut the stiffness reduced nine to ten percent at room temperature, and the behavior of the DMC and DSMC of the beam deflection and rotation in the connection approached that of the behavior of unreduced beam sections (UMC) in fires. The reduced beam-to-column moment connection could withstand a fire of similar intensity compared to that of UMC.

The methodology presented in this study enhances the capabilities of computational methods used to study the effects of various steel members/connections in fires.

Acknowledgements

Part of this study was supported by the National Science Council of Republic of China under grant NSC98-2211-E-006-135-MY3. The steel and the full-scale fire test were supported by China Steel Corporation, Taiwan and Architecture and Building Research Institute (ABRI), Ministry of the Interior, Taiwan, respectively.

References

[1] Usmani AS, Chung YC, Torero JL. How did the WTC towers collapse: a new theory. Fire Safety Journal 2003;38(6):501–33.
[2] Ghojel JI. A new approach to modeling heat transfer in compartment fires. Fire Safety Journal 1998;31:227–37.
[3] Kuldeep P, Howard R Baum. Coupled fire dynamics and thermal response of complex building structures. Proceedings of the Combustion Institute 2005; 30:2255–62.
[4] Ali HM, Senseny PE, Alpert RL. Lateral displacement and collapse of single-story steel frames in uncontrolled fires. Engineering Structures 2004;26: 593–607.
[5] Wickstrom U, Duthinh D, McGrattan K. Adiabatic surface temperature for calculating heat transfer to fires exposed structures. In: 11th international conference on fire science and engineering interflam. 2007.

[6] Duthinh D, McGrattan K, Khaskia A. Recent advances in analysis of structures during fires. Fire Safety Journal 2008;43(2):161–7.
[7] Kodur VKR, Dwaikat MB, Raut N. Macroscopic FE model for tracing the fire response of reinforced concrete srructures. Engineering Structures 2009;31: 2368–79.
[8] Iu CK, Chan SL, Zha XX. Nonlinear pre-fire and post-fire analysis of steel frames. Engineering Structures 2005;27:1689–702.
[9] Silva LS da, Coelho AG. A ductility model for steel connections. Journal of Constructional Steel Research 2001;57:45–70.
[10] Al-Jabri KS, Burgess IW, Plank RJ. Prediction of the degradation of connection characteristics at elevated temperature. Journal of Constructional Steel Research 2004;60:771–81.
[11] Al-Jabri KS. Component-based model of the behaviour of flexible end-plate connections at elevated temperatures. Composite Structures 2004;66:215–21.
[12] Al-Jabri KS, Burgess IW, Plank RJ. Spring-stiffness model for flexible end-plate bare-steel joints in fire. Journal of Constructional Steel Research 2005;61: 1672–91.
[13] Al-Jabri KS, Burgess IW, Lennon T, Plank RJ. Moment–rotation–temperature curves for semi-rigid joints. Journal of Constructional Steel Research 2005;61: 281–303.
[14] Al-Jabri KS, Seibi A, Karrech A. Modelling of unstiffened flush end-plate bolted connections in fire. Journal of Constructional Steel Research 2006;62:151–9.
[15] Newman GM, Robinson JT, Bailey CG. Fire safety design: a new approach to multi-storey steel framed buildings. Ascot Berkshire (UK): SCI Publication p288; 2000.
[16] McGrattan K, Klein B, Hostikka S, Floyd J. Fire dynamics simulator (version 5)—user's guide. NIST Special Publication, P1019-5. 2008.
[17] Chung Hsin-Yang, Lee Chen-Hung, Su Wun-Jie, Lin Rih-Zeng. Application of fire-resistant steel to beam-to-column moment connections at elevated temperatures. Journal of Constructional Steel Research 2010;66:289–303.
[18] European Committee for Standardization (CEN). Design of steel structures: part 1.2: general rules—structural fire design. EN 1993-1-2. Eurocode 3; 1995.
[19] Sarraja M, Burgessa IW, Davisona JB, Plank RJ. Finite element modeling of steel fin plate connections in fire. Fire Safety Journal 2007;42(3):408–15.
[20] Wong MB. Size effect on temperatures of structural steel in fire. Journal of Structural Engineering 2005;131(1):16–20.
[21] Wong MB, Ghojel JI. Sensitivity analysis of heat transfer formulations for insulated structural steel components. Fire Safety Journal 2003;38:187–201.
[22] Engelhardt MD, Winnerberger T, Zekany AJ, Potyraj TJ. Experimental investigation dogbone moment connections. Engineering Journal/Fourth Quarter 1998;128–39.
[23] Chen SJ. Design of ductility seismic moment connections, increased beam section method and reduced beam section method. Steel Structure 2001;1(1).